RESEARCH ARTICLE

Extensive ribosome and RF2 rearrangements during translation termination

Egor Svidritskiy[1], Gabriel Demo[1], Anna B Loveland[1], Chen Xu[2], Andrei A Korostelev[1,2]*

[1]RNA Therapeutics Institute, University of Massachusetts Medical School, Worcester, United States; [2]Biochemistry and Molecular Pharmacology, University of Massachusetts Medical School, Worcester, United States

Abstract Protein synthesis ends when a ribosome reaches an mRNA stop codon. Release factors (RFs) decode the stop codon, hydrolyze peptidyl-tRNA to release the nascent protein, and then dissociate to allow ribosome recycling. To visualize termination by RF2, we resolved a cryo-EM ensemble of *E. coli* 70S•RF2 structures at up to 3.3 Å in a single sample. Five structures suggest a highly dynamic termination pathway. Upon peptidyl-tRNA hydrolysis, the CCA end of deacyl-tRNA departs from the peptidyl transferase center. The catalytic GGQ loop of RF2 is rearranged into a long β-hairpin that plugs the peptide tunnel, biasing a nascent protein toward the ribosome exit. Ribosomal intersubunit rotation destabilizes the catalytic RF2 domain on the 50S subunit and disassembles the central intersubunit bridge B2a, resulting in RF2 departure. Our structures visualize how local rearrangements and spontaneous inter-subunit rotation poise the newly-made protein and RF2 to dissociate in preparation for ribosome recycling.
DOI: https://doi.org/10.7554/eLife.46850.001

Introduction

Ribosomes terminate translation when release factors (RFs) recognize an mRNA stop codon in the A (aminoacyl-tRNA) site (*Brenner et al., 1967*; *Brenner et al., 1965*). Upon stop-codon recognition, the release factor hydrolyzes peptidyl-tRNA in the P site of the large subunit, thus releasing nascent protein from the ribosome (*Capecchi, 1967a*; *Capecchi, 1967b*; *Scolnick et al., 1968*; *Tompkins et al., 1970*). In bacteria, RF1 recognizes UAA or UAG, and RF2 recognizes UAA or UGA codons (*Nakamura et al., 1995*). Following peptide release, RF1 or RF2 must dissociate from the ribosome to allow the ribosome and release factor to recycle. While structural studies have provided snapshots of some peptidyl-tRNA hydrolysis steps (reviewed in *Dunkle and Cate, 2010*; *Korostelev, 2011*; *Ramakrishnan, 2011*; *Rodnina, 2018*; *Youngman et al., 2008*), recent biophysical and biochemical findings suggest a highly dynamic series of termination events (*Adio et al., 2018*; *Indrisiunaite et al., 2015*; *Prabhakar et al., 2017*; *Sternberg et al., 2009*), which have not been structurally visualized.

In the pre-termination (pre-hydrolysis) state, the substrate peptidyl-tRNA resides in a non-rotated (classical) conformation of 70S ribosome, with its anticodon stem loop bound to the mRNA codon in the P site of the small 30S subunit and the 3′-terminal CCA-peptidyl moiety in the P site of the large 50S subunit (*Agrawal et al., 2000*; *Ermolenko et al., 2007*). Cryogenic electron microscopy (cryo-EM) and X-ray studies reveal RF1 or RF2 bound in the A site next to P tRNA (*Klaholz et al., 2003*; *Petry et al., 2005*; *Rawat et al., 2006*; *Rawat et al., 2003*), and provide insight into pre-hydrolysis (*Jin et al., 2010*) and post-hydrolysis states (*Korostelev et al., 2008*; *Korostelev et al., 2010*; *Laurberg et al., 2008*; *Weixlbaumer et al., 2008*). The release factor's codon-recognition domain

(domain 2) binds the stop codon in the 30S decoding center. The catalytic GGQ motif (glycine-gly-cine-glutamine of domain 3) inserts into the 50S peptidyl-transferase center (PTC) adjacent to the CCA end of P-tRNA. Ribosomes retain the non-rotated conformation in RF-bound structures, including those with mutated or post-translationally modified RFs (*Pierson et al., 2016*; *Santos et al., 2013*; *Zeng and Jin, 2018*) or when RFs are perturbed by the termination inhibitor blasticidin S (*Svidritskiy and Korostelev, 2018a*; *Svidritskiy and Korostelev, 2018b*) or by a sense codon in the A site (*Svidritskiy et al., 2018*). The catalytic GGQ loop adopts the same compact conformation comprising a short α-helix in pre-hydrolysis-like and post-hydrolysis structures, as discussed below.

Ribosome and RF dynamics are implicated in post-hydrolysis steps. In *E. coli*, RF1 dissociation is assisted by the non-essential GTPase RF3 (*Freistroffer et al., 1997*; *Koutmou et al., 2014*), whereas RF2 can spontaneously dissociate from the ribosome (*Adio et al., 2018*). RF3 induces rotation of the small subunit relative to the large subunit by ~9 degrees in the absence of RF1 and RF2 (*Ermolenko et al., 2007*; *Zhou et al., 2012*) and stabilizes a 'hybrid' state of deacylated tRNA (P/E) (*Gao et al., 2007*; *Jin et al., 2011*). In the P/E conformation, the anticodon stem loop remains in the 30SS P site, while the elbow and acceptor arm bind the L1 stalk and E (exit) site of the 50S subunit. A recent cryo-EM study (*Graf et al., 2018*) showed that if RF1 is locked on the post-hydrolysis ribosome by antibacterial peptide apidaecin 137 (*Florin et al., 2017*), the ribosome can undergo intersubunit rotation in the presence of both RF1 and RF3. By contrast, biochemical experiments showed that locking RF1 on the ribosome by inactivating its catalytic motif (GGQ->GAQ) prevented RF1 recycling by RF3 from the pre-hydrolysis ribosome (*Koutmou et al., 2014*), echoing the deficiency of mutant RF2 (GGQ->GAQ) in stimulating GTP hydrolysis by RF3 (*Zavialov et al., 2002*). These and other (*Adio et al., 2018*) observations indicate that peptidyl-tRNA hydrolysis is critical for RF dissociation, likely due to propensity of deacylated tRNA for exiting the P site and sampling the P/E hybrid state (*Moazed and Noller, 1989*) via spontaneous intersubunit rotation (*Cornish et al., 2008*). Nevertheless, RF3 is dispensable for growth of *Escherichia coli* (*Grentzmann et al., 1994*; *Mikuni et al., 1994*), and its expression is not conserved in bacteria (*Leipe et al., 2002*). For example, RF3 is not present in the thermophilic model organisms of the *Thermus* and *Thermatoga* genera and in infectious *Chlamydiales* and *Spirochaetae*. This means that both RF1 and RF2 are capable of performing a complete round of termination independently of RF3. Indeed, recent Förster Resonance Energy Transfer (FRET) studies demonstrate spontaneous RF1 and RF2 dissociation after peptidyl-tRNA hydrolysis (*Prabhakar et al., 2017*), coupled with transient RF sampling of the rotated ribosomes (*Adio et al., 2018*). The structural basis for RF dissociation, however, remains incompletely understood because RFs have not been structurally visualized on ribosomes with rearranged/rotated subunits in the absence of RF3 and inhibitors.

In this work, we used ensemble cryo-EM, as described earlier (*Abeyrathne et al., 2016*; *Loveland et al., 2017*), employing 3D maximum likelihood classification/sorting of particle images (*Lyumkis et al., 2013*; *Scheres, 2010*; *Scheres et al., 2007*) to visualize the structural dynamics of RF2 on the 70S ribosome (*Figure 1*, *Figure 1—figure supplement 1*, *Figure 1—figure supplement 2* and *Figure 1—figure supplement 3*). The structures capture RF2 and tRNA in distinct 70S conformational states (*Table 1*). They reveal an unexpected rearrangement of the catalytic GGQ loop, which suggests that RF2 helps direct nascent protein out of the ribosome. Our findings reconcile biophysical observations and, together with other structural studies, allow a reconstruction of the termination course by RF2, from initial binding to dissociation.

Results and discussion

We formed a termination complex using *E. coli* 70S ribosomes and RF2 to catalyze the hydrolysis of substrate N-formyl-methionyl-tRNA^{fMet} (fMet-tRNA^{fMet}) bound to mRNA carrying an AUG codon in the P site and a UGA stop codon in the A site. Although the stop codon is placed immediately after the start codon, unlike in cellular mRNAs, such model termination complexes have been successfully used in numerous structural, biochemical and biophysical studies (*Adio et al., 2018*; *Casy et al., 2018*; *Koutmou et al., 2014*; *Kuhlenkoetter et al., 2011*; *Laurberg et al., 2008*; *Pallesen et al., 2013*; *Pierson et al., 2016*; *Shi and Joseph, 2016*; *Sternberg et al., 2009*). Indeed, under the conditions used for cryo-EM sample preparation in this work, RF2 supports hydrolysis of fMet-tRNA^{fMet} and release of fMet (*Figure 1—figure supplement 4*), demonstrating activity of the ribosome and RF2 in our sample. Maximum-likelihood classification of cryo-EM data in FREALIGN (*Lyumkis et al.,*
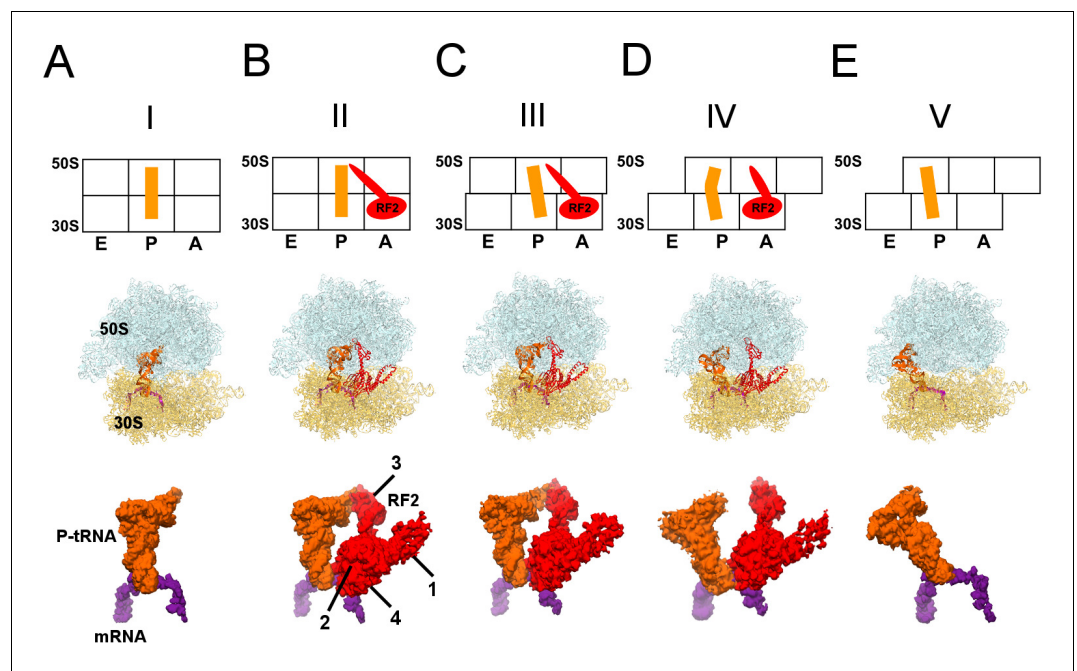
Figure 1. Cryo-EM Structures I to V. Panels A-E show for each structure: *upper row:* a schematic of the conformations of the 70S ribosome, tRNA and RF2, with ribosomal subunits (50S and 30S) and A, P and E sites labeled; *middle row:* structures with RF2 shown in red, tRNA^{fMet} in orange, 30S subunit in yellow, 50S subunit in cyan and mRNA in purple; *lower row:* cryo-EM density for mRNA, tRNA and RF2, colored as in the middle row. Domains of RF2 are labeled in panel B, illustrating the codon-recognition superdomain (domains 2 and 4) and catalytic domain (3).

DOI: https://doi.org/10.7554/eLife.46850.002

The following figure supplements are available for figure 1:

Figure supplement 1. Maximum-likelihood classification strategies to obtain the final maps and state occupancies (shown as percentages of particles for each classification).
DOI: https://doi.org/10.7554/eLife.46850.003

Figure supplement 2. Global and local resolution of Structures I-V.
DOI: https://doi.org/10.7554/eLife.46850.004

Figure supplement 3. A representative micrograph of the 70S•RF2 sample showing ribosome particles.
DOI: https://doi.org/10.7554/eLife.46850.005

Figure supplement 4. RF2 mediates formyl-methionine release from 70S ribosomes.
DOI: https://doi.org/10.7554/eLife.46850.006

2013) yielded five structures at average resolutions of 3.3 Å to 4.4 Å (*Table 2*; *Figure 1*). The structures differ by the degrees of intersubunit rotation and 30S head rotation (swivel), and are consistent with the following termination stages: pre-termination (i.e., no RF2; Structure I); peptidyl-tRNA

Table 1. Cryo-EM structures obtained from a single sample of the 70S•RF2 complex.

	I	II	III	IV	V
tRNA and RF2 occupancy	P-tRNA	P-tRNA, RF2	P-like (L5) tRNA, RF2	P/E-like (L1) tRNA, RF2	P/E tRNA
30S (body) rotation	1.6˚	1.6˚	4.9˚	7.4˚	6.8˚
30S head rotation (swivel)	2.0˚	1.4˚	1.7˚	2.8˚	6.0˚
Resolution (FSC = 0.143)	3.3 Å	3.3 Å	3.7 Å	4.4 Å	3.4 Å

DOI: https://doi.org/10.7554/eLife.46850.007

Table 2. Data collection and refinement statistics for cryo-EM Structures I-V.

STRUCTURE	I	II	III	IV	V
PDB ID	6OFX	6OG7	6OGF	6OGG	6OGI
EMD code	20048	20052	20056	20057	20058
Data collection					
EM equipment	FEI Titan Krios				
Voltage (kV)	300				
Detector	K2 summit				
Pixel size (Å)	1.33				
Electron dose (e⁻/Å²)	29.4				
Defocus range (μm)	– 0.5 – 1.8				
Reconstruction					
Software	Frealign v9.11				
Number of particles in final map	102,723	62,029	28,549	5,881	63,383
Final resolution (Å)	3.3	3.3	3.7	4.4	3.4
Average sharpening B factor (Å²)	-30	-26	-17	-4	-30
Structure Refinement					
Model Fitting	Chimera/Pymol				
Refinement					
Software	RSRef/Phenix				
Correlation Coefficient,cc_mask [*]	0.83	0.84	0.84	0.76	0.82
Real-space R-factor [†]	0.25	0.23	0.22	0.25	0.25
Validation (proteins)					
MolProbity Score [‡]	2.22	2.34	2.42	2.26	2.24
Clash score, all atoms [‡]	17.4	17.4	16.5	15.1	16.3
Poor rotamers (%) [‡]	0.4	0.7	0.7	0.6	0.5
Favored/allowed rotamers (%) [‡]	99.6	99.3	99.3	99.4	99.5
Ramachandran-plot statistics					
Outlier (%) [‡]	0	0.6	0.8	0.0	0.4
Favored (%) [‡]	92.2	88.1	82.3	89.0	90.7
R.m.s. deviations [†,§]					
Bond length (Å)	0.008	0.006	0.006	0.006	0.009
Bond angle (°)	1.064	0.892	0.922	0.848	1.113
Validation (RNA)					
Good sugar puckers (%) [‡]	99.7	99.8	99.8	99.8	99.8
Good backbone conformation (%) [‡]	82.9	84.6	85.0	85.0	82.0

[*]from Phenix

[†]from RSRef

[§]root-mean-square deviations

[#] RNA backbone suites that fall into recognized rotamer conformations defined by MolProbity

DOI: https://doi.org/10.7554/eLife.46850.008

hydrolysis by RF2 (Structure II); tRNA exit from the PTC (Structure III); destabilization of the catalytic domain of RF2 (Structure IV); and post-termination (i.e., after RF2 dissociates; Structure V).

Pre-termination-like Structure I contains tRNA in the P site with its 3′-CCA end positioned in the peptidyl transferase center (*Figure 1A*). Although the tRNA is likely partially or completely
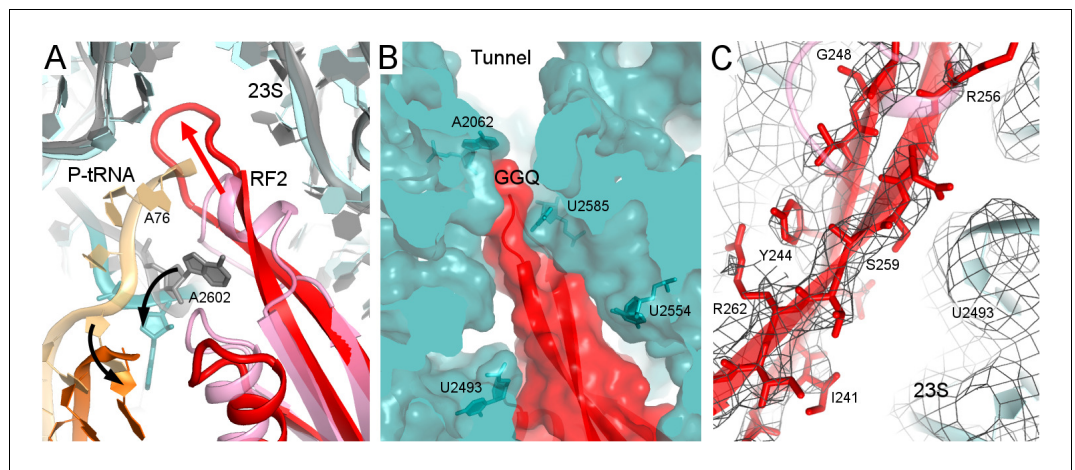
Figure 2. Rearrangement of the catalytic domain of RF2 upon tRNA displacement from the PTC. (**A**) Rearrangements of RF2 in Structure II (RF2 in red, P-tRNA in orange and 23S in cyan) in comparison with the canonical 70S•RF2 conformation (X-ray structure: *Korostelev et al., 2008*; RF2 in pink, P-tRNA in light orange, 23S in gray). Arrows show rearrangements for RF2 (red), tRNA acceptor arm and 23S nucleotide A2602 (black). The superposition was achieved by structural alignment of 23S rRNA. (**B**) The GGQ region of RF2 forms a long β-hairpin that reaches into the constriction of the peptide tunnel (at A2062) and thus plugs the tunnel. Nucleotides of 23S rRNA and the GGQ motif are labeled. (**C**) Cryo-EM density for the β-hairpin formed by the GGQ region. Residues of RF2 and 23S rRNA (also shown in panel B for reference) are labeled.
DOI: https://doi.org/10.7554/eLife.46850.009

The following figure supplements are available for figure 2:

Figure supplement 1. Rearrangements of PTC nucleotides (cyan) upon formation of the β-hairpin structure by the catalytic region of RF2 (red; Structure II is shown).
DOI: https://doi.org/10.7554/eLife.46850.010

Figure supplement 2. Cryo-EM density (mesh) shows that the tip of the GGQ loop of RF2 is poorly ordered (gray model) when the catalytic domain adopts the β-hairpin conformation (red; Structure II is shown).
DOI: https://doi.org/10.7554/eLife.46850.011

deacylated due to the action of RF2, the tRNA and ribosome conformations closely resemble those in pre-termination aminoacyl- and peptidyl-tRNA complexes (*Adio et al., 2018*; *Cornish et al., 2008*; *Jin et al., 2010*; *Polikanov et al., 2014*). The 30S subunit adopts a conformation similar to crystal structures of non-rotated ribosomes with or without RFs (*Jin et al., 2010*; *Korostelev et al., 2008*; *Korostelev et al., 2006*; *Korostelev et al., 2010*; *Laurberg et al., 2008*; *Selmer et al., 2006*; *Weixlbaumer et al., 2008*), and exhibits a slight ~1.5˚ rotation relative to the 70S•RF2 crystal structure formed with the UGA stop codon (*Weixlbaumer et al., 2008*).

RF2 is bound in Structures II to IV (*Figure 1B–D*). The 70S intersubunit rotation ranges from ~1.5˚ in Structure II to ~7.5˚ in Structure IV (*Table 1*). This nearly full range of rotation is typical of translocation complexes with tRNA (*Agirrezabala et al., 2008*; *Agirrezabala et al., 2012*; *Dunkle et al., 2011*; *Fischer et al., 2010*; *Julián et al., 2008*) and elongation factor G (EF-G) (*Brilot et al., 2013*; *Chen et al., 2013*; *Frank and Agrawal, 2000*; *Gao et al., 2009*; *Pulk and Cate, 2013*; *Tourigny et al., 2013*; *Zhou et al., 2013*).

The most well-resolved 3.3 Å resolution Structure II (*Figure 1B*) accounts for the largest population of RF2-bound ribosome particles in the sample (*Table 2*), consistent with stabilization of the non-rotated 30S states by RF2 observed in FRET studies (*Casy et al., 2018*; *Prabhakar et al., 2017*; *Sternberg et al., 2009*). The overall extended conformation of RF2 resembles that seen in published 70S•RF2 structures (*Korostelev et al., 2008*; *Weixlbaumer et al., 2008*) with its codon-recognition superdomain (domains 2 and 4; *Figure 1B*) bound to the UGA stop codon in the decoding center of the 30S subunit and its catalytic domain 3 inserted into the peptidyl-transferase center.

Structure II features RF2 with a dramatically rearranged catalytic loop, coinciding with the lack of density for the CCA end of the P tRNA. In previous pre- and post-hydrolysis-like structures, the P-tRNA CCA end binds the PTC, and RF2 forms a compact catalytic loop (residues 245–258). In
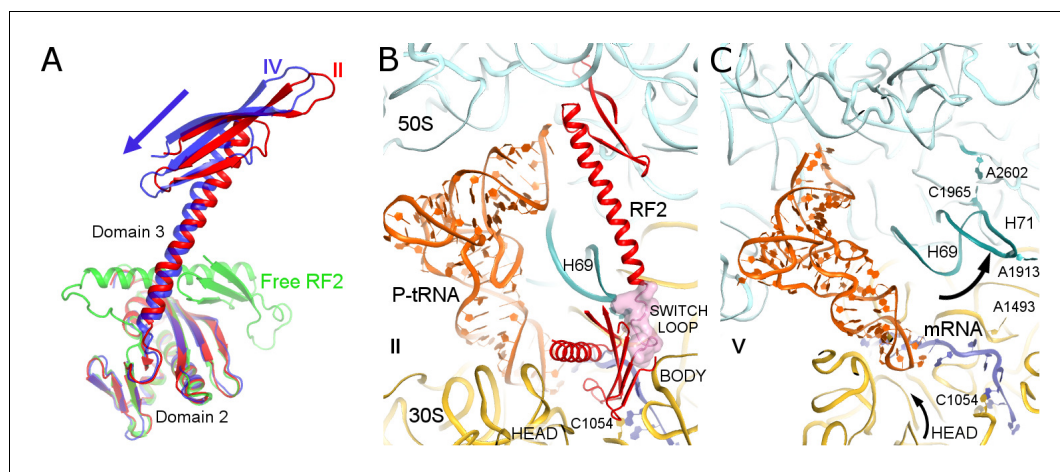
Figure 3. Differences in conformations of RF2 and helix 69 of 23S rRNA in Structures II, IV and V. (**A**) RF2 in Structures II (red) and IV (blue) in comparison with the crystal structure of isolated (free) RF2 (green, PDB 1GQE [*Vestergaard et al., 2001*]). The arrow shows the direction of domain three repositioning from Structure II to IV to free RF2. Structures were aligned by superposition of domain 2. (**B**) Interactions of H69 (teal) with the switch loop (pink surface) of RF2 in Structure II (RF2 in red, P-tRNA in orange, 50S in cyan and 30S in yellow). Domains 2 and 3 of RF2, head and body domains of the 30S subunit and nucleotides A1913 (at H69) and C1054 (head) are labeled. (**C**) In Structure V, dissociation of H69 from the decoding center and packing on H71 next to A2602 disassembles intersubunit bridge B2a. The structure is colored as in panel B. View in panels B and C is rotated by ~180° relative to panel **A**.

DOI: https://doi.org/10.7554/eLife.46850.012

The following figure supplement is available for figure 3:

Figure supplement 1. Structure alignments show that the disengaged H69 in Structure V (teal) is incompatible with the extended (red, Structure II) and compact (pink, PDB 1GQE [*Vestergaard et al., 2001*]) conformations of RF2 due to steric hindrance.

DOI: https://doi.org/10.7554/eLife.46850.013

---

these previous structures, the catalytic ^{250}GGQ^{252} motif resides at the tip of a short α-helix, adjacent to the terminal tRNA nucleotide A76 (*Figure 2A*, light shades; (*Jin et al., 2010*; *Korostelev et al., 2008*; *Laurberg et al., 2008*; *Weixlbaumer et al., 2008*). The α-helical region is held in place by A2602 of 23S ribosomal RNA (rRNA), which is critical for termination efficiency (*Amort et al., 2007*; *Polacek et al., 2003*). In Structure II, however, the catalytic loop adopts an extended β-hairpin conformation that reaches ~10 Å deeper into the peptide tunnel (*Figure 2A–B*). To accommodate the extended β-hairpin, nucleotides G2505 and U2506 of 23S rRNA are shifted to widen the PTC (*Figure 2—figure supplement 1A*). The center of the β-hairpin occupies the position normally held by A76 of P tRNA (*Figure 2A*). The lack of density for the CCA moiety thus suggests that the 3′ end of P tRNA is at least partially released from the PTC. Indeed, formation of the β-hairpin and release of the CCA moiety is accompanied by a slight shift in the P-tRNA acceptor arm away from the PTC and by ~160° rotation of nucleotide A2602 to form a Hoogsteen base pair with C1965 at helix 71 of 23S rRNA (*Figure 2A* and *Figure 2Figure 2—figure supplement 1B*). The cryo-EM map shows strong density for the extended β strands (*Figure 2C*), but weaker density for the GGQ residues at the tip of the hairpin, consistent with conformational heterogeneity of the flexible glycine backbone (*Figure 2—figure supplement 2*). Nevertheless, the tip of the β-hairpin plugs the narrowest region of the peptide tunnel at A2062 of 23S rRNA (*Figure 2B*). Thus, Structure II appears to represent a previously unseen post-peptide-release state with deacyl-tRNA dissociating from the PTC.

In Structure III (*Figure 1C*), a 5° rotation of the 30S subunit shifts the tRNA elbow by ~10 Å along protein L5 toward the E site. As a result, the P-tRNA acceptor arm pulls further out of the 50S P site, and the end of the acceptor arm helix points at helix α7 of RF2 near positively charged Lys 282 and Lys 289. The CCA moiety remains unresolved. The 5° intersubunit rotation also causes a slight 2° rotation of RF2 domain 3 relative to domain 2, but the overall conformation of RF2 remains similar to that in Structure II, with the tip of the extended β-hairpin plugging the peptide exit tunnel.
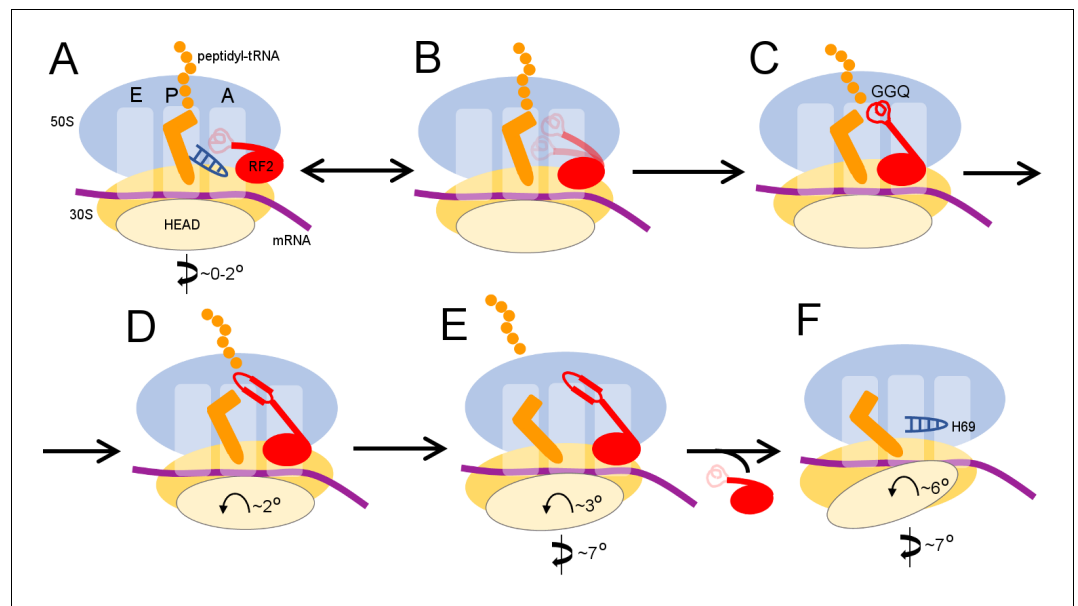
Figure 4. Scheme of the termination mechanism.
DOI: https://doi.org/10.7554/eLife.46850.014

In Structure IV, the 30S subunit is rotated 7.5° and the P-tRNA elbow is bound to the L1 stalk, an interaction normally observed with the P/E or E tRNA (*Dunkle et al., 2011*; *Korostelev et al., 2006*; *Selmer et al., 2006*). Unlike P/E tRNA, however, the acceptor arm is oriented between the 50S P and E sites (*Figure 1D*), suggesting that the tRNA adopts a transient state on its way toward the hybrid P/E conformation. This transition coincides with an ~3° rotation (swivel) of the 30S head, characteristic of intermediate stages of tRNA and mRNA translocation (*Abeyrathne et al., 2016*; *Ratje et al., 2010*). The codon-recognition superdomain of RF2 in its canonical conformation moves with the 30S subunit, causing the catalytic domain to shift by ~5 Å from its position in Structure II (*Figure 3A*). Indeed, reduced density for the catalytic domain and domain 1, which bridges the 30S and 50S subunits at the A site periphery (*Figure 1B*), suggests that intersubunit rotation has destabilized RF2. In Structure IV, therefore, RF2 appears to be poised for dissociation and collapsing toward the compact conformation adopted by free RFs (*Figure 3A*) (*JCSG, 2005*; *Shin et al., 2004*; *Vestergaard et al., 2001*; *Zoldák et al., 2007*).

Structure V is incompatible with RF2 binding and provides further insights into RF2 dissociation. The rotated 70S•tRNA structure resembles hybrid P/E states, with the acceptor arm of tRNA directed toward the E site of 50S (*Figure 1E*). However, the central intersubunit bridge B2a—formed by helix 69 (H69, nt. 1906–1924) of 23S rRNA—is disassembled (*Figure 3B–C*). In RF-bound structures (including Structures I to IV, above), the tip of H69 (at nt 1913) locks into the decoding center in a termination-specific arrangement (*Korostelev et al., 2008*; *Korostelev et al., 2010*; *Laurberg et al., 2008*; *Weixlbaumer et al., 2008*). H69 interacts with the switch loop of RFs, where the codon-recognition superdomain connects to catalytic domain 3 (e.g., Structure II, *Figure 3B*). This interaction directs the catalytic domain toward the PTC (*Korostelev et al., 2010*; *Laurberg et al., 2008*) and thus defines the efficiency and accuracy of release factors (*Svidritskiy and Korostelev, 2018a*). In Structure V, however, H69 is disengaged from the decoding center and moved ~15 Å toward the large subunit to pack against H71 near A2602 (nt 1945–1961; *Figure 3C*). The new position of H69 would clash with extended or compact conformations of RF2 (*Figure 3—figure supplement 1*), if the release factor had remained bound to the decoding center.

Release of RF2 also appears to be coupled to rotation (swivel) of the 30S head domain. In RF2-bound structures, the conserved codon-recognition ^{205}SPF^{207} motif (serine-proline-phenylalanine of domain 2) of RF2 interacts with the stop codon and the 30S head near bulged nucleotide C1054 of 16S rRNA. In Structure V, a 6° rotation of the 30S head shifts the position of C1054 by 5 Å from its position in RF2-bound Structure IV, consistent with disassembly of RF2 contacts. The disruption of
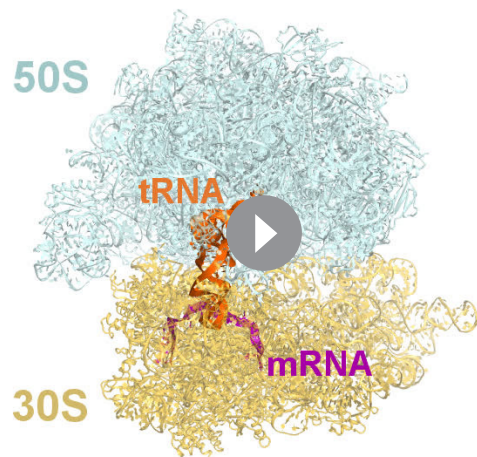
Animation 1. An animation showing transitions between the structures of the 70S ribosome upon interaction with RF2.
DOI: https://doi.org/10.7554/eLife.46850.015

decoding-center interactions due to repositioning of H69 and head swivel therefore explain the absence of RF2 in Structure V.

Mechanism of translation termination by RF2

Our termination structures allow us to reconstruct a dynamic pathway for termination (*Figure 4* and *Animation 1*) and reconcile biophysical and bio-chemical findings (*Adio et al., 2018*; *Casy et al., 2018*; *Prabhakar et al., 2017*; *Sternberg et al., 2009*). Recent structural studies revealed compact RF conformations on non-rotated 70S ribo-somes (*Fu et al., 2018*; *Svidritskiy and Korostelev, 2018a*) that suggest how RFs open at early stages of codon recognition (*He and Green, 2010*; *Hetrick et al., 2009*; *Trappl and Joseph, 2016*). The short-lived transition from compact to open conformation(s) lasts tens of milliseconds (*Fu et al., 2018*), and compact RF2 conformations were not captured in our sample. Compact RF2 was also visualized by cryo-EM on the 70S ribosome in the presence of truncated mRNA and alternative rescue factor A (ArfA)

(*Demo et al., 2017*; *James et al., 2016*), suggesting a conserved pathway for initial binding of RFs to non-rotated ribosomes. Together with these recent studies, our work provides an expanded structural view of the termination reaction – from initial codon recognition to peptide release to RF2 dissociation (*Figure 4*).

Termination begins when release factor recognizes a stop codon in the A site of a non-rotated (or slightly rotated) 70S ribosome carrying peptidyl-tRNA (*Figure 4A*). A compact release factor recognizes the stop codon, while its catalytic domain is kept 60 to 70 Å away from the PTC (*Fu et al., 2018*). Separation of the codon-recognition and catalytic functions during initial binding of RF underlies high accuracy of termination (*He and Green, 2010*; *Laurberg et al., 2008*; *Svidritskiy and Korostelev, 2018a*; *Trappl and Joseph, 2016*). Upon binding the decoding center, steric hindrance with P-tRNA forces the RF catalytic domain to undock from domain two and sample the intersubunit space (*Figure 4B*) (discussed in *Svidritskiy and Korostelev, 2018a*). The ribosome remains non-rotated because peptidyl-tRNA bridges the P sites of 30S and 50S subunits. Interactions between the switch loop of RF and the decoding center and H69 direct the catalytic domain into the PTC. The GGQ catalytic loop is placed next to the scissile ester bond of peptidyl-tRNA and stabilized by A2602 (*Jin et al., 2010*; *Laurberg et al., 2008*), so that the Gln backbone amide of the GGQ motif can catalyze peptidyl-tRNA hydrolysis (*Figure 4C*) (*Korostelev et al., 2008*; *Santos et al., 2013*). These ribosome and RF2 rearrangements complete the first stage of termination leading to peptidyl-tRNA hydrolysis—an irreversible step that separates the newly made protein from P-site tRNA and prevents further elongation.

To be recycled, the ribosome must release the nascent protein and RF. The deacylated CCA end of the tRNA exits the 50S P site, which allows movement of A2602. No longer stabilized by the tRNA and A2602, the GGQ loop reorganizes into an extended β-hairpin that blocks the peptide tunnel (Structure II), thus biasing the diffusion of nascent peptide toward the exit of the peptide tunnel at the surface of the 50S subunit (*Figure 4D*). Furthermore, the exit of the CCA end from the P site supports formation of the P/E-tRNA hybrid conformation via spontaneous intersubunit rotation (Structures III and IV), which is also essential for translocation of tRNA-mRNA (reviewed in *Ling and Ermolenko, 2016*; *Noller et al., 2017*). The large counter-clockwise rotation of the small subunit destabilizes the catalytic domain of RF2 (Structure IV), so that it begins to collapse toward domain 2 bound to the 30S subunit (*Figure 4E*). Rotation of the 30S head and detachment of H69 from the decoding center force dissociation of RF2 from the A site of the 30S subunit (Structure V, *Figure 4F*).

Remarkably similar extents of intersubunit rotation and head rotation were observed in recent RF1-bound 70S structures formed with RF3•GDPNP in the presence of apidaecin (which stalls RF1 on the ribosome). In the presence of stalled RF1, however, the intersubunit bridge remains attached to the decoding center (*Graf et al., 2018*). Thus, the ribosome samples globally similar rotation states with RF1 and RF2, with or without RF3. RF3 stabilizes the rotated state (*Ermolenko et al., 2007*; *Gao et al., 2007*; *Jin et al., 2011*; *Zhou et al., 2012*) to promote RF release. However, the role of RF3 in termination is dispensable because intersubunit rotation is an inherent— that is spontaneous and thermally driven—property of the ribosome (*Cornish et al., 2008*). Cold sensitivity of RF3-deletion strains (*Nichols et al., 2011*; *O'Connor, 2015*) perhaps manifests the dependence on RF3 due to perturbation of the intersubunit dynamics at lower temperatures. In the fully rotated state, the post-termination ribosome becomes a substrate for subunit dissociation by EF-G and recycling factor RRF (*Agrawal et al., 2004*; *Dunkle et al., 2011*; *Fu et al., 2016*; *Prabhakar et al., 2017*). Structure V is consistent with structural studies showing ribosome recycling factor (RRF) bound to ribosomes with a dislodged intersubunit bridge B2a (*Borovinskaya et al., 2007*; *Pai et al., 2008*), which helps split the ribosome into subunits. Translation termination and recycling of the release factors and the ribosome therefore rely on the spontaneous ribosome dynamics (*Adio et al., 2018*; *Cornish et al., 2008*; *Ermolenko et al., 2007*; *Prabhakar et al., 2017*; *Sternberg et al., 2009*), coupled with local rearrangements of the universally conserved elements of the peptidyl-transferase and decoding centers.

Materials and methods

Key resources table

Reagent type (species) or resource	Designation	Source or reference	Identifiers	Additional information
Strain, strain background (*Escherichia coli*)	*Escherichia coli* MRE600	(*Cammack and Wade, 1965*)	ATCC 29417	
Strain, strain background (*Escherichia coli*)	*Escherichia coli* BLR (DE3)	Novagen		
Recombinant protein	C-terminally His-tagged K-12 *E. coli* RF2	(*Demo et al., 2017*)		
Recombinant DNA reagent	*E. coli* RF2 plasmid (vector pET24b)	(*Demo et al., 2017*)		
Chemical compound, drug	*E. coli* tRNA^{fMet}	Chemical Block		
Chemical compound, drug	[^{35}S]-methionine	Perkin Elmer	NEG709A500UC	
Chemical compound, drug	Biodegradable Scintillation Cocktail	Econo-Safe		
Sequence-based reagent	RNA GGCAAGGAGG UAAAAAUGUGAAAAAAA	IDT		
Software, algorithm	PHENIX	(*Adams et al., 2002*)	https://www.phenix-online.org/	
Software, algorithm	CNS	(*Brunger, 2007*)	http://cns-online.org/v1.2/	
Software, algorithm	PyMOL	(*DeLano, 2002*)	https://pymol.org/2/	
Software, algorithm	Chimera	(*Pettersen et al., 2004*)	https://www.cgl.ucsf.edu/chimera/	
Software, algorithm	Bsoft	(*Heymann and Belnap, 2007*)	https://lsbr.niams.nih.gov/bsoft/	
Software, algorithm	Frealign	(*Lyumkis et al., 2013*)	http://grigorefflab.janelia.org/frealign	

Continued on next page

Continued

Reagent type (species) or resource	Designation	Source or reference	Identifiers	Additional information
Software, algorithm	cisTEM	(*Grant et al., 2018*)	https://cistem.org/	
Software, algorithm	MolProbity	(*Chen et al., 2010*)	http://molprobity.biochem.duke.edu/	
Software, algorithm	RSRef	(*Chapman, 1995*; *Korostelev et al., 2002*)	http://www.sb.fsu.edu/~rsref/	
Software, algorithm	SerialEM	(*Mastronarde, 2005*)	http://bio3d.colorado.edu/SerialEM/	
Other	Holey-carbon grids QUANTIFOIL R 2/1, Cu 200	Quantifoil Micro Tools		
Other	Vitrobot MK4	FEI		
Other	Titan Krios microscope	FEI		
Other	K2 Summit camera	Gatan		

Preparation of the 70S termination complex with RF2

N-terminally His6-tagged release factor 2 (RF2) from *E. coli* K12 strain was overexpressed in *E. Coli* BLR (DE3) (Novagen) and purified as described for RF1 (*Svidritskiy and Korostelev, 2018a*). Due to overexpression, RF2 is likely incompletely methylated (or unmethylated) at Q252 of the catalytic GGQ motif (*Dinçbas-Renqvist et al., 2000*), which together with the K12-specific T246 residue, renders RF2 catalytically slower (*Dinçbas-Renqvist et al., 2000*), yet functionally and structurally similar to the post-translationally modified release factors (*Korostelev et al., 2008*; *Pierson et al., 2016*; *Weixlbaumer et al., 2008*; *Zeng and Jin, 2018*). *E. coli* tRNA[fMet] (Chemical Block) was aminoacylated as described (*Lancaster and Noller, 2005*). 70S ribosomes were prepared from *E. coli* (MRE600) as described (*Svidritskiy and Korostelev, 2018a*). Ribosomes were stored in the ribosome-storage buffer (20 mM Tris-HCl, pH 7.0; 100 mM NH$_4$Cl; 12.5 mM MgCl$_2$; 0.5 mM EDTA; 6 mM β-mercaptoethanol) at –80°C. A model mRNA fragment, containing the Shine-Dalgarno sequence and a spacer to position the AUG codon in the P site and the UGA stop codon in the A site (GGC AAG GAG GUA AAA <u>AUG UGA</u> AAAAAA), was synthesized by IDT.

The 70S•mRNA•fMet-tRNA[fMet] complex with RF2 was assembled in vitro by mixing 400 nM 70S ribosome (all concentrations are specified for the final pre-termination solution) with 12 μM mRNA in buffer containing 20 mM Tris-acetate (pH 7.0), 100 mM NH$_4$OAc, 15 mM Mg(OAc)$_2$. After incubation for two minutes at 37°C, 600 nM fMet-tRNA[fMet] was added and incubated for five minutes at 37°C. The Mg(OAc)$_2$ concentration was adjusted to 10 mM by adding an equal volume of buffer (20 mM Tris-acetate (pH 7.0), 100 mM NH$_4$OAc, 5 mM Mg(OAc)$_2$) at room temperature. The release reaction was started by adding an equal volume of 4 μM RF2 (in 20 mM Tris, 100 mM NH$_4$OAc, 10 mM Mg(OAc)$_2$) to the pre-termination solution, yielding the following final concentrations: 0.2 μM 70S, 6 μM mRNA, 0.3 μM fMet-tRNA[fMet], and 2 μM RF2. The solution was incubated for 30 min at room temperature prior to grid preparation and plunging.

The activity of *E. coli* RF2 was tested in an in vitro assay that measures the release of formyl-methionine from the 70S ribosome bound with [35S]-fMet-tRNA[fMet] in the P site, as described (*Svidritskiy and Korostelev, 2018a*). Pre-termination complex was prepared using 0.2 μM *E. coli* 70S ribosomes (all concentrations are for the final reaction mixture upon initiation of the release reaction), 6 μM mRNA and 0.3 μM [35S]-fMet-tRNA[fMet] ([35S]-methionine from Perkin Elmer). An aliquot (4.5 μl) of the pre-termination complex was quenched in 30 μl of 0.1 M HCl to represent the zero-time point. Pre-termination complex was split into two tubes. 5 μl of 20 μM RF2 was added to 45 μl of the pre-termination complex in one tube, yielding 2 μM RF2 in the reaction. Buffer without RF2 was added to the second tube to test spontaneous (RF2-independent) hydrolysis of [35S]-fMet-tRNA[fMet]. After 6, 15, 90 s, and 6, 15, 30, 60 and 150 min, 5 μl aliquots were quenched in 30 μl of 0.1 M HCl. Samples were extracted with ethylacetate, and the amount of released [35S]-labeled N-formyl-methionine was measured using a scintillation counter (Beckman Coulter, Inc) in 3.5 ml of Econo-Safe scintillation cocktail (RPI). All measurements were performed twice (*Figure 1—figure supplement 4*) and time progress data were analyzed and visualized using GraphPad Prizm 7.01.

Cryo-EM and image processing

Holey-carbon grids (QUANTIFOIL R 2/1, Cu 200, Quantifoil Micro Tools) were coated with carbon and glow discharged with 20 mA with negative polarity for 60 s in a PELCO easiGlow glow discharge unit. 2.8 µl of the 70S•mRNA•fMet-tRNA^{fMet}•RF2 complex was applied to the grids. Grids were blotted at blotting force 10 for 4 s at room temperature, 100% humidity, and plunged into liquid ethane using a Vitrobot MK4 (FEI). Grids were stored in liquid nitrogen.

A dataset of 1,069,908 particles was collected on a Titan Krios (FEI) microscope (operating at 300 kV) equipped with a K2 Summit camera system (Gatan), with −0.5 to −1.8 µm defocus. Multi-shot data collection was performed by recording six exposures per hole, using SerialEM (*Mastronarde, 2005*) with beam-image shift. Coma-free alignment was performed using a built-in function. 'Coma vs. Image Shift' from the Calibration menu was used for dynamic beam-tilt compensation, based on image shifts for each exposure. Multi-hole/multi-shot configuration was selected from 'Multiple Record Setup Dialog' to dynamically adjust the beam tilt. Backlash-corrected compensation was applied to each stage movement at the target stage position to reduce mechanical stage drift. 7287 movies were collected. Each exposure (32 frames per movie) was acquired with continuous frame streaming, yielding a total dose of 29.4 e$^-$/Å^2. The nominal magnification was 105,000 and the calibrated super-resolution pixel size at the specimen level was 0.667 Å. 6972 movies were selected after discarding those with defects due to ice or image recording. Movies were processed using IMOD (*Kremer et al., 1996*) and binned to pixel size 1.334 Å (termed unbinned or 1 × binned). Movies were motion-corrected, and frame averages were calculated using all 32 frames within each movie (*Figure 1—figure supplement 3*), after multiplying by the corresponding gain reference. cisTEM (*Grant et al., 2018*) was used to determine defocus values for each resulting frame average and for particle picking. The stack and particle parameter files were assembled in cisTEM with the binnings of 1×, 2×, 4×, and 6× (box size of 624 for a non-binned stack).

Data were processed essentially as described in our recent work (*Loveland et al., 2017*) and shown in *Figure 1—figure supplement 1*. FrealignX was used for particle alignment, refinement, and final reconstruction steps, and Frealign v9.11 was used for 3D classification steps (*Lyumkis et al., 2013*). The 6×-binned image stack (1,069,908 particles) was initially aligned to a ribosome reference without release factor and tRNA (PDB 5J4D) (*Svidritskiy et al., 2016*) using 3 cycles of mode 3 (global search) alignment, including data from 20 Å to 300 Å resolution. Subsequently, the 6×-binned stack was refined using mode 1 (3 cycles) to align particles in the 15- to 300 Å resolution range. Using the 4×-binned image stack, the particles were successively refined using mode one by gradually increasing the high-resolution limit to 12- and 10 Å (three cycles for each resolution limit). 3D density reconstruction was obtained using 60% of particles with highest scores. The map contained density for the P-tRNA, mRNA, and RF2.

Data classification was performed using a spherical focused mask with a 45 Å radius, centered roughly between the A-site finger (nucleotides 870–910 of 23S rRNA), protein L11, and peptidyl transferase center. The mask covered most of the ribosomal A site and part of the P site. The particle stack was classified into 16 classes, using the high-resolution limit of 10 Å. The classification resulted in five RF2-containing classes, six classes with tRNA alone (two classes represented Structures I and V), three classes of the 70S ribosome without tRNA, and two classes of the 50S subunit alone. All classes were subsequently reconstructed using the unbinned stack. Three strongest classes with RF2 were merged and extracted from the unbinned stack, and subclassified into 10 classes without masking, using a high-resolution limit of 8 Å. This classification yielded Structure II, four maps that were merged to obtain Structure III, a map with a rotated 70S•RF2 conformation (used for further classification to obtain Structure IV), a lower-resolution map similar to Structure II, and three junk (poorly resolved) classes. The class corresponding to the rotated 70S•RF2 conformation was extracted from the unbinned substack and further classified into three classes using a 25 Å radius spherical-focused mask roughly centered at the elbow of tRNA (high-resolution limit at 12 Å), yielding Structure IV. All final classes were reconstructed in FrealignX (1×-binning) using 95% of particles with highest scores.

The resulting reconstructions varied from 3.3 Å (Structure II) to 4.4 (Structure IV) Å average resolution (Fourier Shell Correlation (FSC) = 0.143). Cryo-EM reconstructions were B-factor sharpened in bfactor.exe (part of Frealign distribution) using different B-factor values (suggested by bfactor.exe) and then used for model building and structure refinements. B-factor from −50 to −100 Å^2 was also

used for initial refinements and to visualize higher-resolution details. FSC curves were calculated by FrealignX for even and odd particle half-sets (*Figure 1—figure supplement 2*). FSC between the final models and maps, self and cross-validation FSC (*Figure 1—figure supplement 2*) calculated using Phenix (*Adams et al., 2010*) demonstrate good overall agreement between the structural models and maps, similarly to those in previous work (*Brown et al., 2017*). Blocres (part of Bsoft package v1.9.1; *Heymann and Belnap, 2007*) was used to calculate local-resolution maps (*Figure 1—figure supplement 2*).

Model building and refinement

Cryo-EM structures of *E. coli* 70S•ArfA•RF2 complex (*Demo et al., 2017*) excluding ArfA, and the 70S•fMet-tRNA^{fmet} complex with EF-Tu ternary complex (*Loveland et al., 2017*) and improved structure of S2 (*Loveland and Korostelev, 2018*), excluding the ternary complex, were used to create initial models for structure refinement. Chimera (*Pettersen et al., 2004*) was used for fitting the 50S subunit, 30S head, 30S body, mRNA, tRNA, and RF2 domains. Local model fitting was performed in PyMOL (*DeLano, 2002*).

Each structural model was refined by real-space simulated-annealing refinement using atomic electron scattering factors in RSRef, as described (*Svidritskiy et al., 2014*) (*Chapman, 1995*; *Korostelev et al., 2002*). Secondary-structure restraints, comprising hydrogen-bonding restraints for ribosomal proteins and base-pairing restraints for RNA molecules, were employed as described (*Korostelev et al., 2008*). Refinement parameters, such as the relative weighting of stereochemical restraints and experimental energy term, were optimized to produce the stereochemically optimal models that closely agree with the corresponding maps. In the final stage, the structures were refined using Phenix (phenix.real_space_refine) (*Adams et al., 2010*), followed by a round of refinement in RSRef, applying harmonic restraints to preserve protein backbone geometry. B-factors were refined in Phenix. The refined structural models closely agree with the corresponding maps and have good stereochemical parameters, characterized by low deviation from ideal bond lengths and angles, low numbers of protein-backbone outliers and other robust structure-quality statistics, as shown in *Table 2*. Structure quality was validated using MolProbity (*Chen et al., 2010*).

Structure superpositions were performed in PyMOL. For structural comparisons, the distances and angles were calculated in PyMOL and Chimera, respectively. To calculate an angle of the 30S subunit rotation between two 70S structures, the 23S rRNAs were aligned using PyMOL, and the angle between 16S rRNAs body domains (all nucleotide residues excluding 925–1390) was measured in Chimera. To calculate an angle of the 30S-head rotation (swivel) between two 70S structures, the 16S rRNAs of the 30S body were aligned using PyMOL, and the angle between the 16S rRNA residues 925–1390 was measured in Chimera. Ribosome conformations (30S body/subunit rotation and 30S head rotation) for Structures I through V were compared with the crystal structure of the 70S•RF2 complex formed with the UGA stop codon (*Weixlbaumer et al., 2008*).

Unsharpened cryo-EM maps (direct output from Frealign) were deposited in EMDB (Structure I – EMD-20048, Structure II – EMD-20052, Structure III – EMD-20056, Structure IV – EMD-20057, Structure V – EMD-20058). The corresponding PDB models were deposited in RCSB (PDB codes: 6OFX, 6OG7, 6OGF, 6OGG, 6OGI respectively). Figures were prepared in PyMOL.

Additional information

Funding

Author contributions

Egor Svidritskiy, Conceptualization, Data curation, Formal analysis, Validation, Investigation, Visualization, Methodology, Writing—review and editing, Assembled the ribosome complexes, Performed biochemistry, Collected and processed cryo-EM data, Modeled and refined structural models; Gabriel Demo, Data curation, Formal analysis, Investigation, Methodology, Purified ribosome subunits and RF2, Assisted with structure refinements; Anna B Loveland, Formal analysis, Methodology, Assisted with data processing; Chen Xu, Methodology, Implemented multiple-shot (per hole) data acquisition, Optimized data collection; Andrei A Korostelev, Conceptualization, Resources, Formal analysis, Supervision, Funding acquisition, Validation, Investigation, Writing—original draft, Project administration, Writing—review and editing, Supervised the project, Assisted with modeling and structure refinements, Wrote the manuscript with input from co-authors

Author ORCIDs

Gabriel Demo (ID) https://orcid.org/0000-0002-5472-9249
Anna B Loveland (ID) https://orcid.org/0000-0001-9172-7747
Andrei A Korostelev (ID) https://orcid.org/0000-0003-1588-717X

Decision letter and Author response

Decision letter https://doi.org/10.7554/eLife.46850.038
Author response https://doi.org/10.7554/eLife.46850.039

Additional files

Supplementary files

• Transparent reporting form
DOI: https://doi.org/10.7554/eLife.46850.016

Data availability

Structural models have been deposited in PDB under the accession codes 6OFX, 6OG7, 6OGF, 6OGG, 6OGI. Cryo-EM data have been deposited to EMDB under the accession codes EMD-20048, EMD-20052, EMD-20056, EMD-20057, EMD-20058.

The following datasets were generated:

Author(s)	Year	Dataset title	Dataset URL	Database and Identifier
Svidritskiy E, Demo G, Loveland AB, Xu C, Korostelev AA	2019	Non-rotated ribosome (Structure I)	http://www.rcsb.org/structure/6OFX	Protein Data Bank, 6OFX
Svidritskiy E, Demo G, Loveland AB, Xu C, Korostelev AA	2019	Non-rotated ribosome (Structure I)	https://www.ebi.ac.uk/pdbe/entry/emdb/EMD-20048	Electron Microscopy Data Bank, EMD-200 48
Svidritskiy E, Demo G, Loveland AB, Xu C, Korostelev AA	2019	70S termination complex with RF2 bound to the UGA codon. Non-rotated ribosome with RF2 bound (Structure II)	http://www.rcsb.org/structure/6OG7	Protein Data Bank, 6OG7
Svidritskiy E, Demo G, Loveland AB, Xu C, Korostelev AA	2019	70S termination complex with RF2 bound to the UGA codon. Partially rotated ribosome with RF2 bound (Structure III)	http://www.rcsb.org/structure/6OGF	Protein Data Bank, 6OGF
Svidritskiy E, Demo G, Loveland AB, Xu C, Korostelev AA	2019	70S termination complex with the UGA stop codon. Rotated ribosome conformation (Structure	http://www.rcsb.org/structure/6OGI	Protein Data Bank, 6OGI

			V)		
Svidritskiy E, Demo G, Loveland AB, Xu C, Korostelev AA	2019	70S termination complex with RF2 bound to the UGA codon. Rotated ribosome with RF2 bound (Structure IV)	http://www.rcsb.org/structure/6OGG	Protein Data Bank, 6OGG
Svidritskiy E, Demo G, Loveland AB, Xu C, Korostelev AA	2019	70S termination complex with RF2 bound to the UGA codon. Non-rotated ribosome with RF2 bound (Structure II)	https://www.ebi.ac.uk/pdbe/entry/emdb/EMD-20052	Electron Microscopy Data Bank, EMD-200 52
Svidritskiy E, Demo G, Loveland AB, Xu C, Korostelev AA	2019	70S termination complex with RF2 bound to the UGA codon. Partially rotated ribosome with RF2 bound (Structure III)	https://www.ebi.ac.uk/pdbe/entry/emdb/EMD-20056	Electron Microscopy Data Bank, EMD-200 56
Svidritskiy E, Demo G, Loveland AB, Xu C, Korostelev AA	2019	70S termination complex with RF2 bound to the UGA codon. Rotated ribosome with RF2 bound (Structure IV)	https://www.ebi.ac.uk/pdbe/entry/emdb/EMD-20057	Electron Microscopy Data Bank, EMD-200 57
Svidritskiy E, Demo G, Loveland AB, Xu C, Korostelev AA	2019	70S termination complex with the UGA stop codon. Rotated ribosome conformation (Structure V)	https://www.ebi.ac.uk/pdbe/entry/emdb/EMD-20058	Electron Microscopy Data Bank, EMD-200 58

References

Abeyrathne PD, Koh CS, Grant T, Grigorieff N, Korostelev AA. 2016. Ensemble cryo-EM uncovers inchworm-like translocation of a viral IRES through the ribosome. *eLife* **5**:e14874. DOI: https://doi.org/10.7554/eLife.14874, PMID: 27159452

Adams PD, Grosse-Kunstleve RW, Hung LW, Ioerger TR, McCoy AJ, Moriarty NW, Read RJ, Sacchettini JC, Sauter NK, Terwilliger TC. 2002. PHENIX: building new software for automated crystallographic structure determination. *Acta Crystallographica Section D Biological Crystallography* **58**:1948–1954. DOI: https://doi.org/10.1107/S0907444902016657, PMID: 12393927

Adams PD, Afonine PV, Bunkóczi G, Chen VB, Davis IW, Echols N, Headd JJ, Hung LW, Kapral GJ, Grosse-Kunstleve RW, McCoy AJ, Moriarty NW, Oeffner R, Read RJ, Richardson DC, Richardson JS, Terwilliger TC, Zwart PH. 2010. *PHENIX*: a comprehensive Python-based system for macromolecular structure solution. *Acta Crystallographica Section D Biological Crystallography* **66**:213–221. DOI: https://doi.org/10.1107/S0907444909052925, PMID: 20124702

Adio S, Sharma H, Senyushkina T, Karki P, Maracci C, Wohlgemuth I, Holtkamp W, Peske F, Rodnina MV. 2018. Dynamics of ribosomes and release factors during translation termination in *E. coli. eLife* **7**:e34252. DOI: https://doi.org/10.7554/eLife.34252, PMID: 29889659

Agirrezabala X, Lei J, Brunelle JL, Ortiz-Meoz RF, Green R, Frank J. 2008. Visualization of the hybrid state of tRNA binding promoted by spontaneous ratcheting of the ribosome. *Molecular Cell* **32**:190–197. DOI: https://doi.org/10.1016/j.molcel.2008.10.001, PMID: 18951087

Agirrezabala X, Liao HY, Schreiner E, Fu J, Ortiz-Meoz RF, Schulten K, Green R, Frank J. 2012. Structural characterization of mRNA-tRNA translocation intermediates. *PNAS* **109**:6094–6099. DOI: https://doi.org/10.1073/pnas.1201288109, PMID: 22467828

Agrawal RK, Spahn CM, Penczek P, Grassucci RA, Nierhaus KH, Frank J. 2000. Visualization of tRNA movements on the *Escherichia coli* 70S ribosome during the elongation cycle. *The Journal of Cell Biology* **150**:447–460. DOI: https://doi.org/10.1083/jcb.150.3.447, PMID: 10931859

Agrawal RK, Sharma MR, Kiel MC, Hirokawa G, Booth TM, Spahn CM, Grassucci RA, Kaji A, Frank J. 2004. Visualization of ribosome-recycling factor on the *Escherichia coli* 70S ribosome: functional implications. *PNAS* **101**:8900–8905. DOI: https://doi.org/10.1073/pnas.0401904101, PMID: 15178758

Amort M, Wotzel B, Bakowska-Zywicka K, Erlacher MD, Micura R, Polacek N. 2007. An intact ribose moiety at A2602 of 23S rRNA is key to trigger peptidyl-tRNA hydrolysis during translation termination. *Nucleic Acids Research* **35**:5130–5140. DOI: https://doi.org/10.1093/nar/gkm539, PMID: 17660192

Borovinskaya MA, Pai RD, Zhang W, Schuwirth BS, Holton JM, Hirokawa G, Kaji H, Kaji A, Cate JH. 2007. Structural basis for aminoglycoside inhibition of bacterial ribosome recycling. *Nature Structural & Molecular Biology* **14**:727–732. DOI: https://doi.org/10.1038/nsmb1271, PMID: 17660832

Brenner S, Stretton AO, Kaplan S. 1965. Genetic code: the 'nonsense' triplets for chain termination and their suppression. *Nature* **206**:994–998. DOI: https://doi.org/10.1038/206994a0, PMID: 5320272

Brenner S, Barnett L, Katz ER, Crick FH. 1967. UGA: a third nonsense triplet in the genetic code. *Nature* **213**:449–450. DOI: https://doi.org/10.1038/213449a0, PMID: 6032223

Brilot AF, Korostelev AA, Ermolenko DN, Grigorieff N. 2013. Structure of the ribosome with elongation factor G trapped in the pretranslocation state. *PNAS* **110**:20994–20999. DOI: https://doi.org/10.1073/pnas.1311423110, PMID: 24324137

Brown A, Rathore S, Kimanius D, Aibara S, Bai XC, Rorbach J, Amunts A, Ramakrishnan V. 2017. Structures of the human mitochondrial ribosome in native states of assembly. *Nature Structural & Molecular Biology* **24**:866–869. DOI: https://doi.org/10.1038/nsmb.3464, PMID: 28892042

Brunger AT. 2007. Version 1.2 of the crystallography and NMR system. *Nature Protocols* **2**:2728–2733. DOI: https://doi.org/10.1038/nprot.2007.406, PMID: 18007608

Cammack KA, Wade HE. 1965. The sedimentation behaviour of ribonuclease-active and -inactive ribosomes from Bacteria. *Biochemical Journal* **96**:671–680. DOI: https://doi.org/10.1042/bj0960671, PMID: 5324303

Capecchi MR. 1967a. Polypeptide chain termination in vitro: isolation of a release factor. *PNAS* **58**:1144–1151. DOI: https://doi.org/10.1073/pnas.58.3.1144, PMID: 5233840

Capecchi MR. 1967b. A rapid assay for polypeptide chain termination. *Biochemical and Biophysical Research Communications* **28**:773–778. DOI: https://doi.org/10.1016/0006-291X(67)90384-1, PMID: 6061555

Casy W, Prater AR, Cornish PV. 2018. Operative binding of class I release factors and YaeJ stabilizes the ribosome in the nonrotated state. *Biochemistry* **57**:1954–1966. DOI: https://doi.org/10.1021/acs.biochem.7b00824, PMID: 29499110

Chapman MS. 1995. Restrained real-space macromolecular atomic refinement using a new resolution-dependent electron-density function. *Acta Crystallographica Section a Foundations of Crystallography* **51**:69–80. DOI: https://doi.org/10.1107/S0108767394007130

Chen VB, Arendall WB, Headd JJ, Keedy DA, Immormino RM, Kapral GJ, Murray LW, Richardson JS, Richardson DC. 2010. *MolProbity*: all-atom structure validation for macromolecular crystallography. *Acta Crystallographica Section D Biological Crystallography* **66**:12–21. DOI: https://doi.org/10.1107/S0907444909042073, PMID: 20057044

Chen Y, Feng S, Kumar V, Ero R, Gao YG. 2013. Structure of EF-G-ribosome complex in a pretranslocation state. *Nature Structural & Molecular Biology* **20**:1077–1084. DOI: https://doi.org/10.1038/nsmb.2645, PMID: 23912278

Cornish PV, Ermolenko DN, Noller HF, Ha T. 2008. Spontaneous intersubunit rotation in single ribosomes. *Molecular Cell* **30**:578–588. DOI: https://doi.org/10.1016/j.molcel.2008.05.004, PMID: 18538656

DeLano WL. 2002. The PyMOL Molecular Graphics System. Palo Alto, CA, USA, DeLano Scientific.

Demo G, Svidritskiy E, Madireddy R, Diaz-Avalos R, Grant T, Grigorieff N, Sousa D, Korostelev AA. 2017. Mechanism of ribosome rescue by ArfA and RF2. *eLife* **6**:e23687. DOI: https://doi.org/10.7554/eLife.23687, PMID: 28300532

Dinçbas-Renqvist V, Engström A, Mora L, Heurgué-Hamard V, Buckingham R, Ehrenberg M. 2000. A post-translational modification in the GGQ motif of RF2 from Escherichia coli stimulates termination of translation. *The EMBO Journal* **19**:6900–6907. DOI: https://doi.org/10.1093/emboj/19.24.6900, PMID: 11118225

Dunkle JA, Wang L, Feldman MB, Pulk A, Chen VB, Kapral GJ, Noeske J, Richardson JS, Blanchard SC, Cate JH. 2011. Structures of the bacterial ribosome in classical and hybrid states of tRNA binding. *Science* **332**:981–984. DOI: https://doi.org/10.1126/science.1202692, PMID: 21596992

Dunkle JA, Cate JH. 2010. Ribosome structure and dynamics during translocation and termination. *Annual Review of Biophysics* **39**:227–244. DOI: https://doi.org/10.1146/annurev.biophys.37.032807.125954, PMID: 20192776

Ermolenko DN, Majumdar ZK, Hickerson RP, Spiegel PC, Clegg RM, Noller HF. 2007. Observation of intersubunit movement of the ribosome in solution using FRET. *Journal of Molecular Biology* **370**:530–540. DOI: https://doi.org/10.1016/j.jmb.2007.04.042, PMID: 17512008

Fischer N, Konevega AL, Wintermeyer W, Rodnina MV, Stark H. 2010. Ribosome dynamics and tRNA movement by time-resolved electron cryomicroscopy. *Nature* **466**:329–333. DOI: https://doi.org/10.1038/nature09206, PMID: 20631791

Florin T, Maracci C, Graf M, Karki P, Klepacki D, Berninghausen O, Beckmann R, Vázquez-Laslop N, Wilson DN, Rodnina MV, Mankin AS. 2017. An antimicrobial peptide that inhibits translation by trapping release factors on the ribosome. *Nature Structural & Molecular Biology* **24**:752–757. DOI: https://doi.org/10.1038/nsmb.3439, PMID: 28741611

Frank J, Agrawal RK. 2000. A ratchet-like inter-subunit reorganization of the ribosome during translocation. *Nature* **406**:318–322. DOI: https://doi.org/10.1038/35018597, PMID: 10917535

Freistroffer DV, Pavlov MY, MacDougall J, Buckingham RH, Ehrenberg M. 1997. Release factor RF3 in e.coli accelerates the dissociation of release factors RF1 and RF2 from the ribosome in a GTP-dependent manner. *The EMBO Journal* **16**:4126–4133. DOI: https://doi.org/10.1093/emboj/16.13.4126, PMID: 9233821

Fu Z, Kaledhonkar S, Borg A, Sun M, Chen B, Grassucci RA, Ehrenberg M, Frank J. 2016. Key intermediates in ribosome recycling visualized by Time-Resolved cryoelectron microscopy. *Structure* **24**:2092–2101. DOI: https://doi.org/10.1016/j.str.2016.09.014, PMID: 27818103

Fu Z, Indrisiunaite G, Kaledhonkar S, Shah B, Sun M, Chen B, Grassucci RA, Ehrenberg M, Frank J. 2018. The structural basis for release factor activation during translation termination revealed by time-resolved cryogenic electron microscopy. *bioRxiv*. DOI: https://doi.org/10.1016/j.bpj.2018.11.3090

Gao H, Zhou Z, Rawat U, Huang C, Bouakaz L, Wang C, Cheng Z, Liu Y, Zavialov A, Gursky R, Sanyal S, Ehrenberg M, Frank J, Song H. 2007. RF3 induces ribosomal conformational changes responsible for dissociation of class I release factors. *Cell* **129**:929–941. DOI: https://doi.org/10.1016/j.cell.2007.03.050, PMID: 17540173

Gao YG, Selmer M, Dunham CM, Weixlbaumer A, Kelley AC, Ramakrishnan V. 2009. The structure of the ribosome with elongation factor G trapped in the posttranslocational state. *Science* **326**:694–699. DOI: https://doi.org/10.1126/science.1179709, PMID: 19833919

Graf M, Huter P, Maracci C, Peterek M, Rodnina MV, Wilson DN. 2018. Visualization of translation termination intermediates trapped by the apidaecin 137 peptide during RF3-mediated recycling of RF1. *Nature Communications* **9**:3053. DOI: https://doi.org/10.1038/s41467-018-05465-1, PMID: 30076302

Grant T, Rohou A, Grigorieff N. 2018. *cis*TEM, user-friendly software for single-particle image processing. *eLife* **7**:e35383. DOI: https://doi.org/10.7554/eLife.35383, PMID: 29513216

Grentzmann G, Brechemier-Baey D, Heurgue V, Mora L, Buckingham RH. 1994. Localization and characterization of the gene encoding release factor RF3 in Escherichia coli. *PNAS* **91**:5848–5852. DOI: https://doi.org/10.1073/pnas.91.13.5848, PMID: 8016077

He SL, Green R. 2010. Visualization of codon-dependent conformational rearrangements during translation termination. *Nature Structural & Molecular Biology* **17**:465–470. DOI: https://doi.org/10.1038/nsmb.1766, PMID: 20208546

Hetrick B, Lee K, Joseph S. 2009. Kinetics of stop Codon recognition by release factor 1. *Biochemistry* **48**:11178–11184. DOI: https://doi.org/10.1021/bi901577d, PMID: 19874047

Heymann JB, Belnap DM. 2007. Bsoft: image processing and molecular modeling for electron microscopy. *Journal of Structural Biology* **157**:3–18. DOI: https://doi.org/10.1016/j.jsb.2006.06.006, PMID: 17011211

Indrisiunaite G, Pavlov MY, Heurgué-Hamard V, Ehrenberg M. 2015. On the pH dependence of class-1 RF-dependent termination of mRNA translation. *Journal of Molecular Biology* **427**:1848–1860. DOI: https://doi.org/10.1016/j.jmb.2015.01.007, PMID: 25619162

James NR, Brown A, Gordiyenko Y, Ramakrishnan V. 2016. Translational termination without a stop Codon. *Science* **354**:1437–1440. DOI: https://doi.org/10.1126/science.aai9127, PMID: 27934701

JCSG. 2005. Crystal structure of peptide chain release factor 1 (RF-1) (SMU.1085) from Streptococcus mutans at 2.34 A resolution. *JC.f.S. Genomics*. DOI: https://doi.org/10.2210/pdb1ZBT/pdb

Jin H, Kelley AC, Loakes D, Ramakrishnan V. 2010. Structure of the 70S ribosome bound to release factor 2 and a substrate analog provides insights into catalysis of peptide release. *PNAS* **107**:8593–8598. DOI: https://doi.org/10.1073/pnas.1003995107, PMID: 20421507

Jin H, Kelley AC, Ramakrishnan V. 2011. Crystal structure of the hybrid state of ribosome in complex with the Guanosine triphosphatase release factor 3. *PNAS* **108**:15798–15803. DOI: https://doi.org/10.1073/pnas.1112185108, PMID: 21903932

Julián P, Konevega AL, Scheres SH, Lázaro M, Gil D, Wintermeyer W, Rodnina MV, Valle M. 2008. Structure of ratcheted ribosomes with tRNAs in hybrid states. *PNAS* **105**:16924–16927. DOI: https://doi.org/10.1073/pnas.0809587105, PMID: 18971332

Klaholz BP, Pape T, Zavialov AV, Myasnikov AG, Orlova EV, Vestergaard B, Ehrenberg M, van Heel M. 2003. Structure of the Escherichia coli ribosomal termination complex with release factor 2. *Nature* **421**:90–94. DOI: https://doi.org/10.1038/nature01225, PMID: 12511961

Korostelev A, Bertram R, Chapman MS. 2002. Simulated-annealing real-space refinement as a tool in model building. *Acta Crystallographica Section D Biological Crystallography* **58**:761–767. DOI: https://doi.org/10.1107/S0907444902003402, PMID: 11976486

Korostelev A, Trakhanov S, Laurberg M, Noller HF. 2006. Crystal structure of a 70S ribosome-tRNA complex reveals functional interactions and rearrangements. *Cell* **126**:1065–1077. DOI: https://doi.org/10.1016/j.cell.2006.08.032, PMID: 16962654

Korostelev A, Asahara H, Lancaster L, Laurberg M, Hirschi A, Zhu J, Trakhanov S, Scott WG, Noller HF. 2008. Crystal structure of a translation termination complex formed with release factor RF2. *PNAS* **105**:19684–19689. DOI: https://doi.org/10.1073/pnas.0810953105, PMID: 19064930

Korostelev A, Zhu J, Asahara H, Noller HF. 2010. Recognition of the amber UAG stop Codon by release factor RF1. *The EMBO Journal* **29**:2577–2585. DOI: https://doi.org/10.1038/emboj.2010.139, PMID: 20588254

Korostelev AA. 2011. Structural aspects of translation termination on the ribosome. *RNA* **17**:1409–1421. DOI: https://doi.org/10.1261/rna.2733411, PMID: 21700725

Koutmou KS, McDonald ME, Brunelle JL, Green R. 2014. RF3:gtp promotes rapid dissociation of the class 1 termination factor. *RNA* **20**:609–620. DOI: https://doi.org/10.1261/rna.042523.113, PMID: 24667215

Kremer JR, Mastronarde DN, McIntosh JR. 1996. Computer visualization of three-dimensional image data using IMOD. *Journal of Structural Biology* **116**:71–76. DOI: https://doi.org/10.1006/jsbi.1996.0013, PMID: 8742726

Kuhlenkoetter S, Wintermeyer W, Rodnina MV. 2011. Different substrate-dependent transition states in the active site of the ribosome. *Nature* **476**:351–354. DOI: https://doi.org/10.1038/nature10247, PMID: 21804565

Lancaster L, Noller HF. 2005. Involvement of 16S rRNA nucleotides G1338 and A1339 in discrimination of initiator tRNA. *Molecular Cell* **20**:623–632. DOI: https://doi.org/10.1016/j.molcel.2005.10.006, PMID: 16307925

Laurberg M, Asahara H, Korostelev A, Zhu J, Trakhanov S, Noller HF. 2008. Structural basis for translation termination on the 70S ribosome. *Nature* **454**:852–857. DOI: https://doi.org/10.1038/nature07115, PMID: 18596689

Leipe DD, Wolf YI, Koonin EV, Aravind L. 2002. Classification and evolution of P-loop GTPases and related ATPases. *Journal of Molecular Biology* **317**:41–72. DOI: https://doi.org/10.1006/jmbi.2001.5378, PMID: 11916378

Ling C, Ermolenko DN. 2016. Structural insights into ribosome translocation. *Wiley Interdisciplinary Reviews: RNA* **7**:620–636. DOI: https://doi.org/10.1002/wrna.1354, PMID: 27117863

Loveland AB, Demo G, Grigorieff N, Korostelev AA. 2017. Ensemble cryo-EM elucidates the mechanism of translation fidelity. *Nature* **546**:113–117. DOI: https://doi.org/10.1038/nature22397, PMID: 28538735

Loveland AB, Korostelev AA. 2018. Structural dynamics of protein S1 on the 70S ribosome visualized by ensemble cryo-EM. *Methods* **137**:55–66. DOI: https://doi.org/10.1016/j.ymeth.2017.12.004, PMID: 29247757

Lyumkis D, Brilot AF, Theobald DL, Grigorieff N. 2013. Likelihood-based classification of cryo-EM images using FREALIGN. *Journal of Structural Biology* **183**:377–388. DOI: https://doi.org/10.1016/j.jsb.2013.07.005, PMID: 23872434

Mastronarde DN. 2005. Automated electron microscope tomography using robust prediction of specimen movements. *Journal of Structural Biology* **152**:36–51. DOI: https://doi.org/10.1016/j.jsb.2005.07.007, PMID: 16182563

Mikuni O, Ito K, Moffat J, Matsumura K, McCaughan K, Nobukuni T, Tate W, Nakamura Y. 1994. Identification of the prfC gene, which encodes peptide-chain-release factor 3 of Escherichia coli. *PNAS* **91**:5798–5802. DOI: https://doi.org/10.1073/pnas.91.13.5798, PMID: 8016068

Moazed D, Noller HF. 1989. Intermediate states in the movement of transfer RNA in the ribosome. *Nature* **342**: 142–148. DOI: https://doi.org/10.1038/342142a0, PMID: 2682263

Nakamura Y, Ito K, Matsumura K, Kawazu Y, Ebihara K. 1995. Regulation of translation termination: conserved structural motifs in bacterial and eukaryotic polypeptide release factors. *Biochemistry and Cell Biology* **73**: 1113–1122. DOI: https://doi.org/10.1139/o95-120, PMID: 8722028

Nichols RJ, Sen S, Choo YJ, Beltrao P, Zietek M, Chaba R, Lee S, Kazmierczak KM, Lee KJ, Wong A, Shales M, Lovett S, Winkler ME, Krogan NJ, Typas A, Gross CA. 2011. Phenotypic landscape of a bacterial cell. *Cell* **144**: 143–156. DOI: https://doi.org/10.1016/j.cell.2010.11.052

Noller HF, Lancaster L, Zhou J, Mohan S. 2017. The ribosome moves: rna mechanics and translocation. *Nature Structural & Molecular Biology* **24**:1021–1027. DOI: https://doi.org/10.1038/nsmb.3505, PMID: 29215639

O'Connor M. 2015. Interactions of release factor RF3 with the translation machinery. *Molecular Genetics and Genomics* **290**:1335–1344. DOI: https://doi.org/10.1007/s00438-015-0994-x, PMID: 25636454

Pai RD, Zhang W, Schuwirth BS, Hirokawa G, Kaji H, Kaji A, Cate JH. 2008. Structural insights into ribosome recycling factor interactions with the 70S ribosome. *Journal of Molecular Biology* **376**:1334–1347. DOI: https://doi.org/10.1016/j.jmb.2007.12.048, PMID: 18234219

Pallesen J, Hashem Y, Korkmaz G, Koripella RK, Huang C, Ehrenberg M, Sanyal S, Frank J. 2013. Cryo-EM visualization of the ribosome in termination complex with apo-RF3 and RF1. *eLife* **2**:e00411. DOI: https://doi.org/10.7554/eLife.00411, PMID: 23755360

Petry S, Brodersen DE, Murphy FV, Dunham CM, Selmer M, Tarry MJ, Kelley AC, Ramakrishnan V. 2005. Crystal structures of the ribosome in complex with release factors RF1 and RF2 bound to a cognate stop Codon. *Cell* **123**:1255–1266. DOI: https://doi.org/10.1016/j.cell.2005.09.039

Pettersen EF, Goddard TD, Huang CC, Couch GS, Greenblatt DM, Meng EC, Ferrin TE. 2004. UCSF chimera–a visualization system for exploratory research and analysis. *Journal of Computational Chemistry* **25**:1605–1612. DOI: https://doi.org/10.1002/jcc.20084, PMID: 15264254

Pierson WE, Hoffer ED, Keedy HE, Simms CL, Dunham CM, Zaher HS. 2016. Uniformity of peptide release is maintained by methylation of release factors. *Cell Reports* **17**:11–18. DOI: https://doi.org/10.1016/j.celrep.2016.08.085, PMID: 27681416

Polacek N, Gomez MJ, Ito K, Xiong L, Nakamura Y, Mankin A. 2003. The critical role of the universally conserved A2602 of 23S ribosomal RNA in the release of the nascent peptide during translation termination. *Molecular Cell* **11**:103–112. DOI: https://doi.org/10.1016/S1097-2765(02)00825-0, PMID: 12535525

Polikanov YS, Steitz TA, Innis CA. 2014. A proton wire to couple aminoacyl-tRNA accommodation and peptide-bond formation on the ribosome. *Nature Structural & Molecular Biology* **21**:787–793. DOI: https://doi.org/10.1038/nsmb.2871

Prabhakar A, Capece MC, Petrov A, Choi J, Puglisi JD. 2017. Post-termination ribosome intermediate acts as the gateway to ribosome recycling. *Cell Reports* **20**:161–172. DOI: https://doi.org/10.1016/j.celrep.2017.06.028, PMID: 28683310

Pulk A, Cate JH. 2013. Control of ribosomal subunit rotation by elongation factor G. *Science* **340**:1235970. DOI: https://doi.org/10.1126/science.1235970, PMID: 23812721

Ramakrishnan V. 2011. *Structural Studies on Decoding, Termination and Translocation in the Bacterial Ribosome*. In: Rodnina M, Wintermeyer W, Green R (Eds). *Ribosomes: Structure, Function, and Dynamics*. Springer.

Ratje AH, Loerke J, Mikolajka A, Brünner M, Hildebrand PW, Starosta AL, Dönhöfer A, Connell SR, Fucini P, Mielke T, Whitford PC, Onuchic JN, Yu Y, Sanbonmatsu KY, Hartmann RK, Penczek PA, Wilson DN, Spahn CM. 2010. Head swivel on the ribosome facilitates translocation by means of intra-subunit tRNA hybrid sites. *Nature* **468**:713–716. DOI: https://doi.org/10.1038/nature09547, PMID: 21124459

Rawat UB, Zavialov AV, Sengupta J, Valle M, Grassucci RA, Linde J, Vestergaard B, Ehrenberg M, Frank J. 2003. A cryo-electron microscopic study of ribosome-bound termination factor RF2. *Nature* **421**:87–90. DOI: https://doi.org/10.1038/nature01224, PMID: 12511960

Rawat U, Gao H, Zavialov A, Gursky R, Ehrenberg M, Frank J. 2006. Interactions of the release factor RF1 with the ribosome as revealed by cryo-EM. *Journal of Molecular Biology* **357**:1144–1153. DOI: https://doi.org/10.1016/j.jmb.2006.01.038, PMID: 16476444

Rodnina MV. 2018. Translation in prokaryotes. *Cold Spring Harbor Perspectives in Biology* **10**:a032664. DOI: https://doi.org/10.1101/cshperspect.a032664

Santos N, Zhu J, Donohue JP, Korostelev AA, Noller HF. 2013. Crystal structure of the 70S ribosome bound with the Q253P mutant form of release factor RF2. *Structure* **21**:1258–1263. DOI: https://doi.org/10.1016/j.str.2013.04.028, PMID: 23769667

Scheres SH, Gao H, Valle M, Herman GT, Eggermont PP, Frank J, Carazo JM. 2007. Disentangling conformational states of macromolecules in 3D-EM through likelihood optimization. *Nature Methods* **4**:27–29. DOI: https://doi.org/10.1038/nmeth992, PMID: 17179934

Scheres SH. 2010. Classification of structural heterogeneity by maximum-likelihood methods. *Methods in Enzymology* **482**:295–320. DOI: https://doi.org/10.1016/S0076-6879(10)82012-9, PMID: 20888966

Scolnick E, Tompkins R, Caskey T, Nirenberg M. 1968. Release factors differing in specificity for terminator codons. *PNAS* **61**:768–774. DOI: https://doi.org/10.1073/pnas.61.2.768, PMID: 4879404

Selmer M, Dunham CM, Murphy FV, Weixlbaumer A, Petry S, Kelley AC, Weir JR, Ramakrishnan V. 2006. Structure of the 70S ribosome complexed with mRNA and tRNA. *Science* **313**:1935–1942. DOI: https://doi.org/10.1126/science.1131127, PMID: 16959973

Shi X, Joseph S. 2016. Mechanism of translation termination: rf1 dissociation follows dissociation of RF3 from the ribosome. *Biochemistry* **55**:6344–6354. DOI: https://doi.org/10.1021/acs.biochem.6b00921, PMID: 27779391

Shin DH, Brandsen J, Jancarik J, Yokota H, Kim R, Kim SH. 2004. Structural analyses of peptide release factor 1 from Thermotoga maritima reveal domain flexibility required for its interaction with the ribosome. *Journal of Molecular Biology* **341**:227–239. DOI: https://doi.org/10.1016/j.jmb.2004.05.055, PMID: 15312775

Sternberg SH, Fei J, Prywes N, McGrath KA, Gonzalez RL. 2009. Translation factors direct intrinsic ribosome dynamics during translation termination and ribosome recycling. *Nature Structural & Molecular Biology* **16**:861–868. DOI: https://doi.org/10.1038/nsmb.1622, PMID: 19597483

Svidritskiy E, Brilot AF, Koh CS, Grigorieff N, Korostelev AA. 2014. Structures of yeast 80S ribosome-tRNA complexes in the rotated and nonrotated conformations. *Structure* **22**:1210–1218. DOI: https://doi.org/10.1016/j.str.2014.06.003, PMID: 25043550

Svidritskiy E, Madireddy R, Korostelev AA. 2016. Structural basis for translation termination on a pseudouridylated stop Codon. *Journal of Molecular Biology* **428**:2228–2236. DOI: https://doi.org/10.1016/j.jmb.2016.04.018, PMID: 27107638

Svidritskiy E, Demo G, Korostelev AA. 2018. Mechanism of premature translation termination on a sense Codon. *Journal of Biological Chemistry* **293**:12472–12479. DOI: https://doi.org/10.1074/jbc.AW118.003232, PMID: 29941456

Svidritskiy E, Korostelev AA. 2018a. Conformational control of translation termination on the 70S ribosome. *Structure* **26**:821–828. DOI: https://doi.org/10.1016/j.str.2018.04.001, PMID: 29731232

Svidritskiy E, Korostelev AA. 2018b. Mechanism of inhibition of translation termination by blasticidin S. *Journal of Molecular Biology* **430**:591–593. DOI: https://doi.org/10.1016/j.jmb.2018.01.007, PMID: 29366636

Tompkins RK, Scolnick EM, Caskey CT. 1970. Peptide chain termination. VII. The ribosomal and release factor requirements for peptide release. *PNAS* **65**:702–708. DOI: https://doi.org/10.1073/pnas.65.3.702, PMID: 4910855

Tourigny DS, Fernández IS, Kelley AC, Ramakrishnan V. 2013. Elongation factor G bound to the ribosome in an intermediate state of translocation. *Science* **340**:1235490. DOI: https://doi.org/10.1126/science.1235490, PMID: 23812720

Trappl K, Joseph S. 2016. Ribosome induces a closed to open conformational change in release factor 1. *Journal of Molecular Biology* **428**:1333–1344. DOI: https://doi.org/10.1016/j.jmb.2016.01.021, PMID: 26827724

Vestergaard B, Van LB, Andersen GR, Nyborg J, Buckingham RH, Kjeldgaard M. 2001. Bacterial polypeptide release factor RF2 is structurally distinct from eukaryotic eRF1. *Molecular Cell* **8**:1375–1382. DOI: https://doi.org/10.1016/S1097-2765(01)00415-4, PMID: 11779511

Weixlbaumer A, Jin H, Neubauer C, Voorhees RM, Petry S, Kelley AC, Ramakrishnan V. 2008. Insights into translational termination from the structure of RF2 bound to the ribosome. *Science* **322**:953–956. DOI: https://doi.org/10.1126/science.1164840, PMID: 18988853

Youngman EM, McDonald ME, Green R. 2008. Peptide release on the ribosome: mechanism and implications for translational control. *Annual Review of Microbiology* **62**:353–373. DOI: https://doi.org/10.1146/annurev.micro.61.080706.093323, PMID: 18544041

Zavialov AV, Mora L, Buckingham RH, Ehrenberg M. 2002. Release of peptide promoted by the GGQ motif of class 1 release factors regulates the GTPase activity of RF3. *Molecular Cell* **10**:789–798. DOI: https://doi.org/10.1016/S1097-2765(02)00691-3, PMID: 12419223

Zeng F, Jin H. 2018. Conformation of methylated GGQ in the peptidyl transferase center during translation termination. *Scientific Reports* **8**:2349. DOI: https://doi.org/10.1038/s41598-018-20107-8, PMID: 29403017

Zhou J, Lancaster L, Trakhanov S, Noller HF. 2012. Crystal structure of release factor RF3 trapped in the GTP state on a rotated conformation of the ribosome. *RNA* **18**:230–240. DOI: https://doi.org/10.1261/rna.031187.111, PMID: 22187675

Zhou J, Lancaster L, Donohue JP, Noller HF. 2013. Crystal structures of EF-G-ribosome complexes trapped in intermediate states of translocation. *Science* **340**:1236086. DOI: https://doi.org/10.1126/science.1236086, PMID: 23812722

Zoldák G, Redecke L, Svergun DI, Konarev PV, Voertler CS, Dobbek H, Sedlák E, Sprinzl M. 2007. Release factors 2 from Escherichia coli and Thermus thermophilus: structural, spectroscopic and microcalorimetric studies. *Nucleic Acids Research* **35**:1343–1353. DOI: https://doi.org/10.1093/nar/gkl696, PMID: 17272297